Removal of Cefdinir from Aqueous Solution Using Nanostructure Adsorbents of TiO_2, SiO_2 and TiO_2/SiO_2: Equilibrium, Thermodynamic and Kinetic Studies

H. Banu Yener*
Ege University, Faculty of Engineering,
Department of Chemical Engineering,
35100 Bornova, Izmir, Turkey

https://doi.org/10.15255/CABEQ.2019.1632

Original scientific paper
Received: March 13, 2019
Accepted: June 13, 2019

The adsorptive removal of cefdinir, an antibiotic, from aqueous solutions on TiO_2, SiO_2 and TiO_2/SiO_2 nanostructures was studied by batch experiments. The SiO_2 particles were obtained from rice husk ash. Investigated were the effects of the solution pH, adsorbent dosage, initial adsorbate concentration, and solution temperature on both cefdinir uptake and removal. The studies suggest that the adsorption of cefdinir on the nanostructures was mainly due to the electrostatic interaction between the ionic adsorbate molecules and charged adsorbent surface sites. The adsorption isotherm data of TiO_2 and SiO_2 fit well to the Langmuir isotherm model and the Freundlich model for TiO_2/SiO_2. The thermodynamic studies indicated favorable and spontaneous occurrence of adsorption. The kinetic data of TiO_2 fitted best with PSO reaction model equation, and was described well by Weber-Morris diffusion model with dominating control mechanism of intraparticle diffusion and limited contribution of internal film diffusion.

Keywords:
TiO_2, SiO_2, TiO_2/SiO_2, adsorption, cefdinir, rice husk ash

Introduction

The pharmaceuticals incompletely metabolized and excreted by humans and animals or released from the pharmaceutical industry during manufacturing increase their amounts in wastewaters. Since they are polar molecules, they are generally soluble in water. Even at trace concentrations (ng L^{-1} or mg L^{-1}) in various water sources, the presence of pharmaceutically active compounds has become a serious environmental and human health concern. Their chemical stability, microbial resistance, biologically active nature through accumulation and synergistic effects with other pharmaceuticals make long-term risks unpredictable[1–3]. Although pharmaceuticals have been released into the environment for several decades, they could not be detected due to their low concentrations. With the development of new and highly sensitive analytical techniques, their detection has been enabled[3,4]. The pharmaceuticals commonly detected in water are anti-inflammatory drugs and analgesics, antacids, lipid-lowering drugs, beta blockers, and antibiotics[3,5,6].

Antibiotics are the most widely used pharmaceuticals for the treatment of various infections in humans and animals. Since most antibiotics are non-biodegradable, they are the most commonly detected pharmaceutical in wastewater. Cefdinir is a third-generation semi-synthetic cephalosporin antibiotic frequently used for the treatment of bacterial infections in adults, children, and infants[7,8]. It has excellent effects against a wide range of Gram-positive and Gram-negative bacteria causing acute respiratory disorders, acute chronic bronchitis, rhinosinusitis, and mild skin infections[8,9]. The biological toxicity, non-biodegradable nature, and high level of suspended components found in the wastewater released during cephalosporin production make them a potential risk to the environment[10].

There are various processes used for the removal of pharmaceuticals from wastewater, such as chemical and biological systems[8,11–14], electrochemical treatment[15–18], advanced oxidation processes[19–24], and adsorption/biosorption[1,4,5,25–32]. The methods possess some drawbacks such as high cost, low removal efficiency, limitations for large-scale applications or formation of hazardous reactive intermediates. Adsorption is one of the most preferred methods, since it provides easy application, is economic and effective, and produces no toxic intermediates. Both the adsorbent properties (surface area, surface charge, porous structure, toxicity, etc.) and adsorption conditions (pH, contact time, initial pharmaceutic concentration, temperature, adsorbent dosage, etc.) determine the yield of the adsorption

*Corresponding author: E-mail: huriye.banu.yener@ege.edu.tr
Tel.: +90 232 3111495, Fax: +90 232 3887776

process. There are various adsorbents such as carbon-based materials[1,4,6,33], resins[30,34,35], zeolite[36], SiO_2[26,37], and TiO_2[38,39] used for the removal of pharmaceuticals and other organic pollutants.

In the present study, cefdinir, as the target antibiotic, was removed by adsorption using TiO_2, SiO_2, and TiO_2/SiO_2. Since TiO_2 and SiO_2 are non-toxic, stable, and inexpensive materials, they have been used in emerging application areas, such as environmental purification. TiO_2 is generally known for its effective photocatalytic property, while SiO_2 is known for its high surface area. In addition to their separate use, in most cases, their hybrid or composite structures have also been used as adsorbents and/or photocatalysts for the removal of different pollutants from aqueous solutions[40–43]. The composites combine the photocatalytic ability of TiO_2 and high surface area of SiO_2, and enhance effectiveness of this combination in the application area. Removal of pollutants from aqueous solution by photocatalytic degradation occurs in two steps: Adsorption of pollutant on photocatalyst surface and/or pores, and then its degradation by photocatalytic reactions. Thus, the adsorption process is a prerequisite step in photocatalytic degradation and should be well defined. There are studies in literature regarding the utilization of TiO_2 or SiO_2 in the removal of different pharmaceuticals from aqueous solution using adsorption[37,44] and/or photocatalytic degradation[21–24]. In addition, there are studies on the removal of different types of cephalosporin from pharmaceutical wastewater using photo-Fenton combined with UV-C irradiation[19], sono-electrochemical catalytic oxidation-driven process[18], biodegradation[8,14], bioadsorption[45], and electrochemical processes[16,17]. However, no studies were found for the use of TiO_2, SiO_2 or their composites in the adsorptive removal of cefdinir.

The main objective of the study was to determine the adsorption performances of TiO_2, SiO_2, and TiO_2/SiO_2 for the removal of cefdinir from aqueous solutions. The TiO_2 used in the present study was synthesized at low temperature, without calcination and without surface modification, as given by Yener and Helvacı[46]. On the other hand, the SiO_2 particles used were obtained from an environmentally friendly agricultural waste of rice husk ash, as described by Yener and Helvacı[46]. Considering all of these issues, the study aimed to clarify the adsorption mechanism using effective, economical, and environmentally friendly adsorbents of TiO_2, SiO_2, and TiO_2/SiO_2 composites. In addition, the study focuses on the determination of the effective conditions for the adsorption of cefdinir, such as pH, initial cefdinir concentration, adsorbent dosage, and temperature.

Experimental

Materials

Titanium tetrachloride ($TiCl_4$, > 99 % purity, Merck) was used as a titanium precursor. Rice husk ash (RHA), kindly supplied by Erdoğanlar Food Industry and Business Company, was used as the silica source. Hydrochloric acid (HCl, 38 %, Merck) and sodium hydroxide (NaOH, 99 %, Merck) were used as pH regulator. Cefdinir of high purity (> 99.9 %) was kindly supplied by Sanovel Pharmaceutical Industry and Business Company. All chemicals were used as received without further purification. For all studies, ultra-pure water obtained from Millipore Direct Q3 system was used.

Synthesis and characterization of the adsorbents

TiO_2, SiO_2, and TiO_2/SiO_2 nanostructures were synthesized applying the same method described in the previously reported study[46]. $TiCl_4$ was used as a titanium precursor, and rice husk ash (RHA) as a silica source. SiO_2 particles were extracted from the RHA under alkaline conditions. TiO_2 particles were synthesized at 95 °C by acid hydrolysis of $TiCl_4$ on the SiO_2 particles with a mass ratio of TiO_2 to SiO_2 of one.

The structural properties of the adsorbents were determined using proper instrumentation and the detailed results were given in the previous work[46]. The morphology of the nanostructures was determined by a field emission gun scanning electron microscope (SEM, FEI QUANTA 250 FEG). The surface charge of the nanostructures was measured using the zeta potential mode of the Malvern Zetasizer Nano ZS. Before the zeta potential measurements, the particles were dispersed in water at different pH, stirred for 3 h, and then allowed to settle by gravity for 24 h.

Adsorption studies

The adsorption performances of the nanostructures for the adsorptive removal of aqueous cefdinir solution were determined by batch studies. The adsorbents (0.1, 0.25, 0.5, 0.75, and 1.5 g L^{-1}) were poured into 250 mL of aqueous cefdinir solution (5, 10, 20, and 40 mg L^{-1}) in a double-walled cylindrical batch reactor. With the addition of the adsorbents, the initial pH of the solution changed insignificantly and remained almost constant throughout the adsorption process. The temperature of the solution was tuned by circulating water at the desired temperature (25, 35, and 50 °C) through the jacket of the reactor. The reactors were covered with aluminum foil to prevent ambient light into the suspen-

sion. The suspension was stirred with magnetic stirrer at a constant stirring rate of 500 rpm in order to hinder the precipitation of the adsorbents for the homogeneity of the suspension. Samples were collected at predetermined time intervals by stopping the stirring. The samples were centrifuged at 6000 rpm for 20 min, and then the supernatant was filtered through a 0.20 mm polytetrafluoroethylene (PTFE) membrane syringe filter. Total sample volume did not exceed 10 % of the initial volume of the cefdinir solution. The cefdinir concentration was analyzed using high performance liquid chromatography (HPLC, Shimadzu 20A) equipped with a UV-Vis detector and an Inertsil ODS-4 column (5 mm, 250 mm x 4.6 mm). The mobile phase with a flow rate of 1.2 mL min^{-1} consisted of 50 % 100 mM NaH_2PO_4 with a pH 2.1, and 50 % acetonitrile. The detection was monitored at 285 nm for cefdinir. The quantitative analyses were performed on the base of the calibration curve with a regression coefficient of 0.998. The calibration curve was obtained by measurement of the standard cefdinir solutions with concentrations of 0.625, 1.25, 2.5, 5, 7.5, 10, and 20 mg L^{-1} using the software package Shimadzu LC Solution version 1.25. All the adsorption experiments were performed at least three times to ensure repeatable results, and the average values were used during evaluation of the data.

The cefdinir uptake per unit mass of the adsorbents at equilibrium, q_e (mg g^{-1}), was determined as:

$$q_e = \frac{C_0 - C_e}{m_{ads}} \cdot V_{sln} \quad (1)$$

where C_0 and C_e are the initial and equilibrium concentrations of cefdinir in solution (mg L^{-1}), m_{ads} is the mass of adsorbent (g), and V_{sln} is the volume of the solution (L). The change in cefdinir uptake with respect to time was determined using Eq. (1) by replacing the equilibrium concentration, C_e, with the concentration at time t, C_t. The adsorption percentage of cefdinir was calculated using Eq. (2);

$$\text{Ads}(\%) = \frac{C_0 - C_e}{C_0} \cdot 100 \quad (2)$$

The effects of solution pH (4, 7, and 10), initial cefdinir concentration (5, 10, 20, and 40 mg L^{-1}), adsorbent dosage (0.1, 0.25, 0.5, 0.75, and 1.5 g L^{-1}), and temperature (25, 35, and 50 °C) on the adsorption performance were studied. Prior to the parametric studies, experiments in the absence of adsorbents were performed to investigate the effects of solution pH and temperature on cefdinir.

A reusability study was also performed in order to determine the reuse of the adsorbent. At the end of the first adsorption process, the adsorbent was separated from the adsorbate solution by centrifugation, washed several times with water, dried at 60 °C, and then reused in the second adsorption process. Washing of the adsorbent continued until no cefdinir was detected in the washing water. The same treatment procedure was applied after each use in the adsorption.

Results and discussion

Characterization of the nanostructures

The morphological and structural properties of the TiO_2, SiO_2, and TiO_2/SiO_2 nanostructures were given in detail in the previous report[46]. The SEM images of the nanostructures are given in Fig. 1. The SEM image of TiO_2 showed spherical agglomerates consisting of interconnected nanofibers. The surface of TiO_2 agglomerates was very smooth due to the small diameter of the nanofibers forming the surface of the sphere. The SEM image of SiO_2 revealed that it had no clear shape, but a highly porous structure. In the SEM image of TiO_2/SiO_2, it was observed that spherical TiO_2 particles covered the surface of SiO_2. The presence of SiO_2 hindered agglomeration and this led to the homogeneous distribution of TiO_2 on the surface of SiO_2. The BSE image given as inset in the SEM image of TiO_2/SiO_2 also indicated the homogeneous distribution of bright colored TiO_2 spheres on dark colored SiO_2 surface. The properties of the nanostructures previously reported are summarized in Table 1. At predefined conditions, TiO_2 and SiO_2 particles were in rutile and amorphous structures, respectively. All of the nanostructures used had mesoporous structure with the external surface area higher than the microporous area. Since TiO_2 particles covered the surface of SiO_2 (Fig. 1), the surface area of the SiO_2 decreased.

The zeta potentials (ZP) of the nanostructures with respect to the pH is given in Fig. 2. Although the ZP of TiO_2 became positive or negative depending on the solution pH, the ZPs of SiO_2 and TiO_2/SiO_2 were found to be negative at the pH range

Table 1 – *Properties of the TiO_2, SiO_2, and TiO_2/SiO_2 nanostructures*

Properties	TiO_2	SiO_2	TiO_2/SiO_2
Crystal structure	Rutile	Amorphous	Rutile/ Amorphous
BET surface area (m^2 g^{-1})	93	433	194
External area* (m^2 g^{-1})	89	402	137
Average pore diameter (nm)	2.90	5.50	6.50
Total pore volume (cm^3 g^{-1})		0.55	0.18

*External areas were calculated by t-plot method.

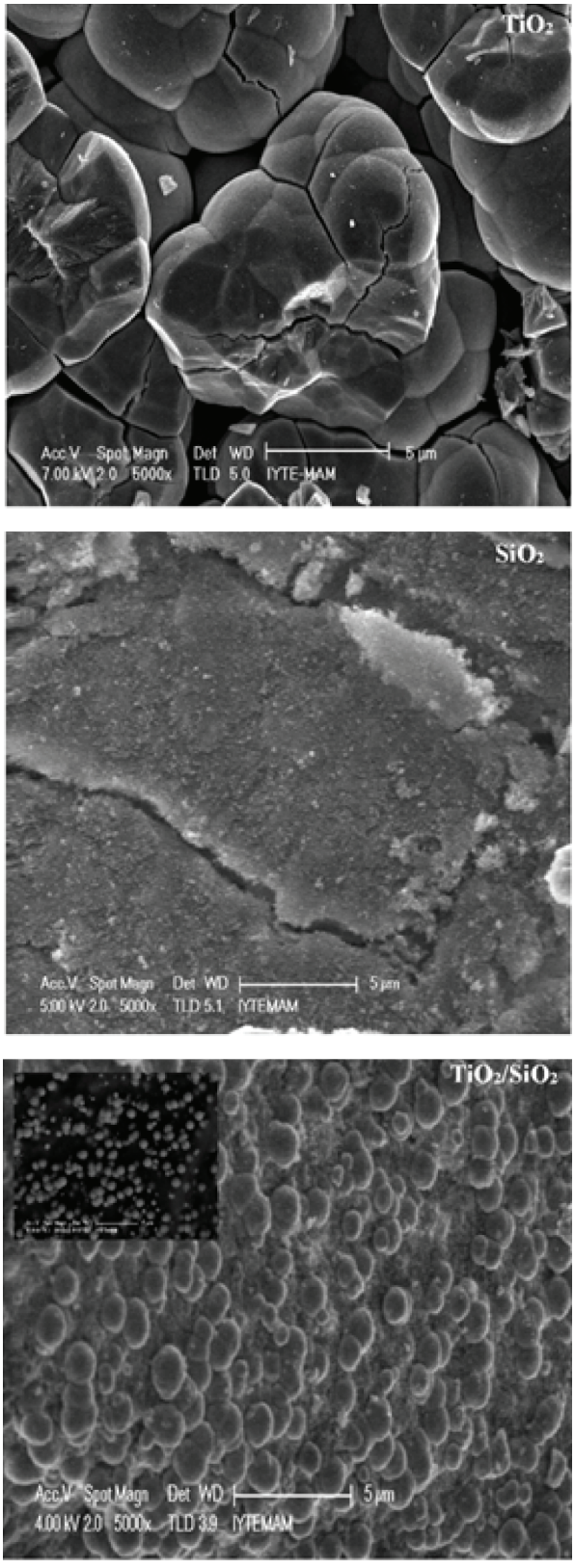

Fig. 1 – *SEM images of the nanostructures (BSE image of TiO_2/SiO_2 as inset)*

studied. The presence of TiO_2 on SiO_2 slightly increased the ZP of TiO_2/SiO_2 compared to that of SiO_2. The isoelectric point of TiO_2 was at 6.7.

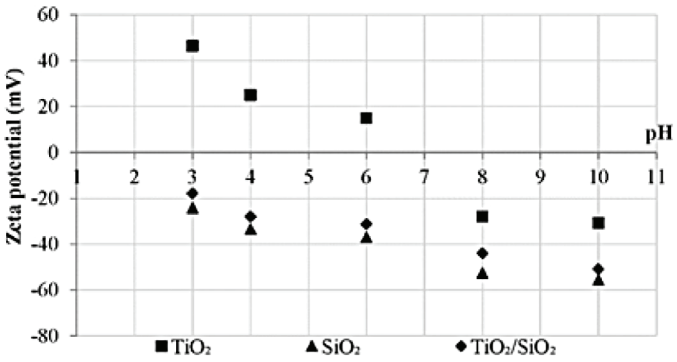

Fig. 2 – *Zeta potentials of the nanostructures as a function of pH*

Effect of solution pH

The adsorption experiments were performed at pHs 4, 7, and 10 by keeping the other adsorption conditions constant at the initial cefdinir concentration of 10 mg L^{-1}, temperature of 25 °C, and adsorbent loading of 1.5, 0.5, and 0.75 g L^{-1} for TiO_2, SiO_2, and TiO_2/SiO_2, respectively. Since the natural pH of the solution was 4, the pHs of 7 and 10 were adjusted using appropriate amounts of aqueous NaOH solution. The slight variation in solution pH throughout the adsorption time was considered negligible. The effect of the solution pH on cefdinir was also studied while there was no adsorbent in the solution. It was observed that the concentration of cefdinir changed unremarkably at pHs 4, 7, and 10 as 1.2, 3.6, and 5.2 %, respectively. The equilibrium cefdinir uptake of the adsorbents as a function of initial solution pH is given in Fig. 3. The cefdinir uptake decreased with the increase in pH for all adsorbents. The pH of the solution affects the surface charge of the adsorbents and the ionic form of the adsorbate, depending on the degree of ionization of the surface groups, and accordingly the adsorption of cefdinir on the nanostructures. Cefdinir has three ionizable groups with pK_a values of 1.9 (–COOH, carboxyl group), 3.3 ($–NH_2$, amino group), and 9.9 (–OH, hydroxyl group)[7,9,47]. Thus, it was expected that the ionization degree of cefdinir would increase with an increase in solution pH. At pH 4, the attractive electrostatic interaction between the ionized cefdinir molecules and positively charged TiO_2 surface (Fig. 2) favored the adsorption process. As the pH of the solution increased from 4 to 7, the surface became less positive, leading to the decrease in cefdinir uptake. Similarly, at pH 10, since the negatively charged surface sites of TiO_2 increased, the attractive interactions between the ionic cefdinir molecules and TiO_2 decreased. In that case, the increase in repulsive electrostatic interactions led to the decrease in adsorption uptake. Due to the negative surface charge of SiO_2 and TiO_2/SiO_2 at the

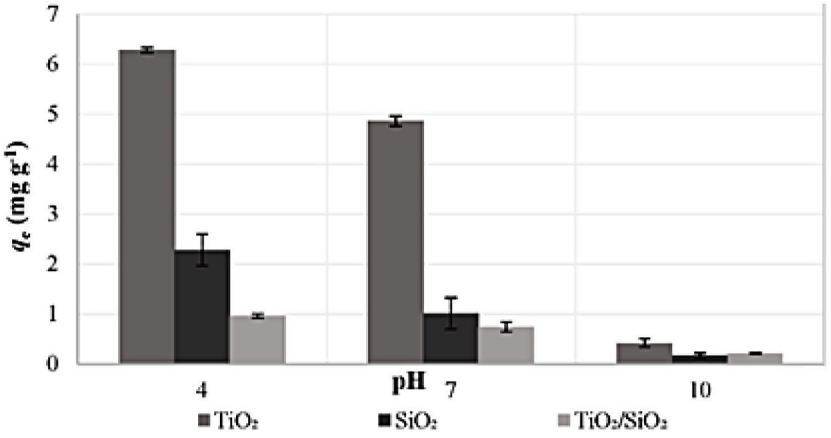

Fig. 3 – *Equilibrium cefdinir uptake on the adsorbents as a function of pH (T = 25 °C, C_0 = 10 mg L^{-1})*

pHs studied, equilibrium uptakes were lower than that of TiO_2. As the pH of the solution increased from 4 to 10, the SiO_2 and TiO_2/SiO_2 adsorbents were more negatively charged, and thus the attractive electrostatic interactions between the ionic cefdinir molecules and the adsorbents became weaker. The trend in equilibrium uptake with respect to the solution pH indicated that the adsorption of cefdinir on the nanostructures was mainly due to the electrostatic interaction between the ionic adsorbate molecules and charged adsorbent surface sites. Since the highest equilibrium uptake was obtained at solution pH 4, further adsorption experiments were performed at this pH.

Adsorption isotherms

The equilibrium adsorption isotherms were used to elucidate the relationship between the amount of adsorbate both in solution and on the adsorbents, at a constant temperature. The equilibrium adsorption isotherms were studied at the initial cefdinir concentrations of 5, 10, 20, and 40 mg L^{-1}, at constant adsorbent loading of 0.1 g L^{-1}, temperature of 25 °C, and solution pH of 4. The change in cefdinir uptake with respect to time indicated that equilibrium had been reached within 10 h.

The adsorption data for the adsorbents as a function of initial cefdinir concentrations were analyzed by Langmuir, Freundlich, and Redlich-Peterson isotherm models. The Langmuir model has two assumptions; fixed number of active sites with the same energy and no interaction between the adsorbate species, that is saturated monolayer adsorption on the adsorbent surface[48,49]. The model is given as[50]:

$$q_e = \frac{Q_m K_L C_e}{1 + K_L C_e} \tag{3}$$

where q_e and C_e are the amount of equilibrium adsorbate uptake (mg g^{-1}), and equilibrium adsorbate concentration in bulk solution (mg L^{-1}), respectively. Q_m is the maximum saturated monolayer adsorption capacity of the adsorbents (mg g^{-1}), and K_L is the equilibrium constant related to the affinity between the adsorbents and adsorbate (L mg^{-1}). The Freundlich model describes the equilibrium data and adsorption characteristics for heterogeneous surface with non-uniform active sites[48,51] as:

$$q_e = K_F C_e^{1/n} \tag{4}$$

where K_F is the Freundlich constant (mg$^{1-1/n}$ L$^{1/n}$ g^{-1}), and n is the Freundlich intensity indicating the magnitude of adsorption driving force or surface heterogeneity[48]. The Redlich-Peterson model is a combination of Langmuir and Freundlich models, and can be used for the adsorption equilibrium over a wide range of adsorbate concentrations. In addition, it can be applied in homogeneous or heterogeneous systems due to its versatility. The model is defined as[48]:

$$q_e = \frac{K_{RP} C_e}{1 + a_{RP} C_e^g} \tag{5}$$

where K_{RP} (L g^{-1}) and a_{RP} (mg L^{-1})$^{-g}$ are the Redlich-Peterson constants, and g is an exponent changing between 0 and 1.

The isotherm model parameters were estimated with a non-linear regression method. The non-linear fitting of each model was evaluated using the average relative deviation (ARD):

$$\mathrm{ARD}(\%) = \frac{1}{n} \sum \left| \frac{y_e - y_c}{y_e} \right| \cdot 100 \tag{6}$$

where y_e and y_c are the experimental and calculated values of cefdinir uptake, and n is the number of samples.

The adsorption isotherms of the adsorbents fitted to the Langmuir, Freundlich, and Redlich-Peter-

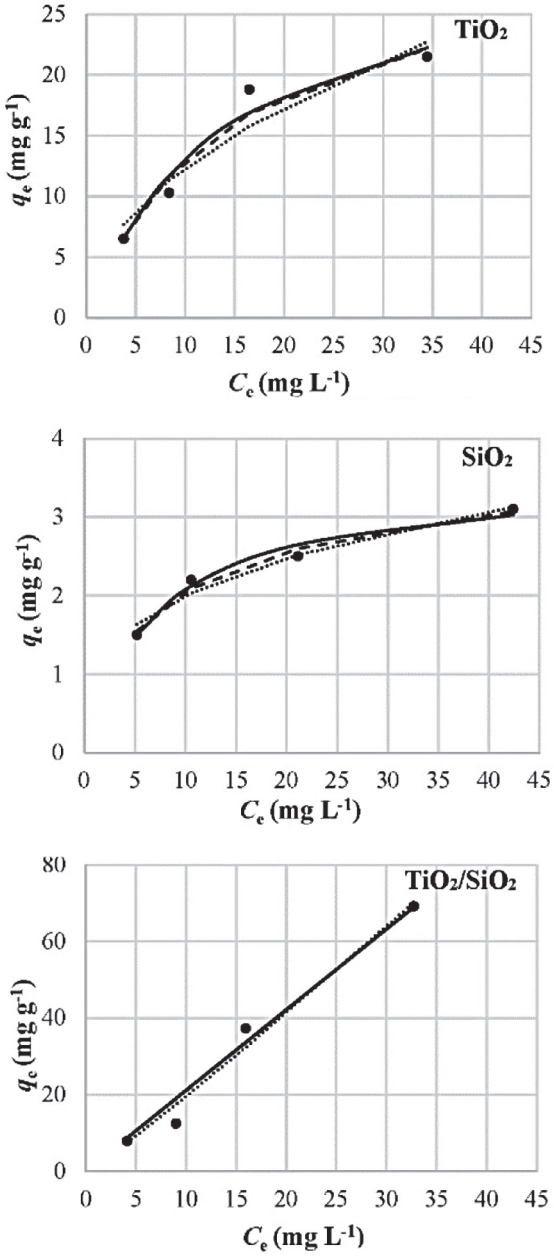

Fig. 4 – *Experimental equilibrium adsorption isotherms (•) fitted to the Langmuir (———), Freundlich (·····) and Redlich-Peterson (--------) models (Adsorbent loadings = 0.1 g L^{-1}, T = 25 °C, pH = 4)*

son models are given in Fig. 4. The model parameters along with the ARD values given in Table 2 showed that Langmuir and Redlich-Peterson models adequately describe the adsorption of cefdinir on TiO_2 and SiO_2. The proximity of exponent *g* to 1 transforms the Redlich-Peterson model to the Langmuir model indicating the monolayer adsorption of cefdinir on TiO_2 and SiO_2 with the homogeneous active sites. The maximum saturated monolayer adsorption capacity of the adsorbents, Q_m of TiO_2 was found to be higher than that of SiO_2 revealing its higher adsorption capacity. On the other hand, both

Table 2 – *Isotherm parameters of Langmuir, Freundlich, and Redlich-Peterson models (Adsorbent loadings = 0.1 g L^{-1}, T = 25 °C, pH = 4)*

	Adsorbents		
	TiO_2	SiO_2	TiO_2/SiO_2
Langmuir			
Q_m (mg g^{-1})	31.36	3.53	11.41
K_L (L mg^{-1})	0.07	0.14	0.0002
R^2	0.959	0.975	0.976
ARD (%)	7.2	3.0	18.0
Freundlich			
K_F (mg$^{1-1/n}$ L$^{1/n}$ g^{-1})	3.98	0.98	1.63
n	2.03	3.22	0.93
R^2	0.914	0.965	0.979
ARD (%)	12.3	4.5	14.9
Redlich-Peterson			
K_{RP} (L g^{-1})	2.22	0.72	4.31
a_{RP} (L^g mg^{-g})	0.07	0.34	1.05
g	1.00	0.88	0.00
R^2	0.960	0.981	0.976
ARD (%)	7.1	3.3	17.8

the model parameters and ARD values indicated that the data of TiO_2/SiO_2 fit best with the Freundlich isotherm model. The linearity in the adsorption isotherm of TiO_2/SiO_2 was also supported by the Freundlich intensity *n,* which was 0.93, close to 1, and by the exponent *g* in Redlich-Peterson, which equaled zero. Thus, cefdinir adsorption on TiO_2/SiO_2 can be described as multilayer adsorption. Since the value of *n*, which indicates the favorable adsorption, was less than 1, poor adsorption occurred on the surface of TiO_2/SiO_2. The variety in the surface property of the TiO_2/SiO_2 due to the presence of both TiO_2 and SiO_2 in the structure with different active sites may have caused the heterogeneous adsorption.

Effect of adsorbent dosage

The adsorption experiments were performed at six different adsorbent dosages (0.1, 0.25, 0.5, 0.75, and 1.5 g L^{-1}). The initial cefdinir concentration of 10 mg L^{-1}, temperature of 25 °C, and solution pH of 4, were kept constant throughout the experiments. The changes in adsorption percentage and cefdinir uptake with respect to the adsorbent dosage are given in Fig. 5. As may be seen in Fig. 5(a), for TiO_2,

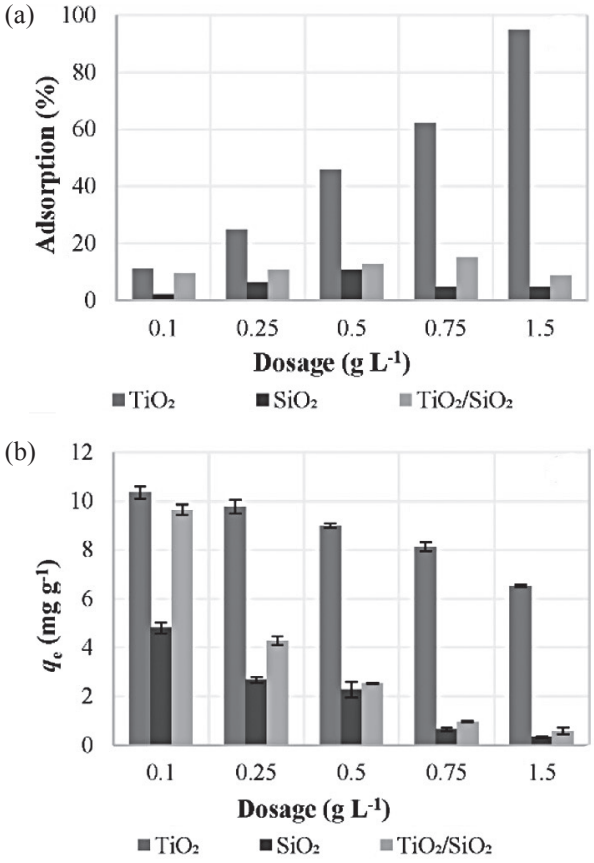

Fig. 5 – *Change in (a) adsorption percentage, and (b) uptake of cefdinir with respect to adsorbent dosage (C_0 = 10 mg L^{-1}, T = 25 °C, pH = 4)*

the adsorption percentage increased with increasing adsorbent dosage, whereas for SiO_2 and TiO_2/SiO_2, it reached a maximum and then decreased. The increase in adsorption percentage was attributed to the increase in active sites at higher dosages[5,26,52,53]. Nevertheless, although the equilibrium uptake was generally expected to be constant and independent of the adsorbent dosage, for all adsorbents studied, the cefdinir uptake decreased with the increase in adsorbent dosage (Fig. 5(b)). In order to elucidate this situation, it can be speculated that the excess amount of adsorbent in the solution may have led to the increase in collision between the particles causing agglomeration followed by a reduction in the uptake capacity[5,25,26,53]. The decrease in equilibrium cefdinir uptake of SiO_2 and TiO_2/SiO_2 with respect to the adsorbent dosage was higher than that of TiO_2. The large sizes of SiO_2 and TiO_2/SiO_2 induced agglomeration and reduction in the surface area, which led to the decrease in adsorption percentage after an adsorbent dosage, and a sharp decrease in uptake. Adsorbent dosages of 1.5, 0.5, and 0.75 g L^{-1} for TiO_2, SiO_2 and TiO_2/SiO_2 nanostructures, respectively, were selected for further studies in order to achieve high cefdinir removal.

Thermodynamics of adsorption

The adsorption mechanisms were predicted with thermodynamic studies conducted at the temperatures of 25, 35, and 50 °C with the adsorbent loadings of 0.1 g L^{-1}, and the initial cefdinir concentrations of 5, 10, 20, and 40 mg L^{-1}. The natural solution pH 4 was kept constant throughout the experiments. The effect of temperature on cefdinir was also studied while there was no adsorbent in the solution. It was found that the concentration of cefdinir unremarkably changed at temperatures 25, 35, and 50 °C as 1.4, 2.4, and 4.4 %, respectively. The thermodynamic properties were determined according to the laws of thermodynamics as:

$$\Delta G^0 = -RT \ln K_c \tag{7}$$

where ΔG^0 is the Gibbs free energy (kJ mol^{-1}), R is the universal gas constant (8.314 J mol^{-1} K^{-1}), T is the absolute temperature (K), and K_c is the dimensionless equilibrium constant. The relation between the enthalpy, ΔH^0 (kJ mol^{-1}) and entropy, ΔS^0 (J mol^{-1}) changes of adsorption, and ΔG^0 is expressed as:

$$\Delta G^0 = \Delta H^0 - T\Delta S^0 \tag{8}$$

The van't Hoff equation is obtained using Eqs. (7) and (8), as

$$\ln K_c = \frac{-\Delta H^0}{R}\frac{1}{T} + \frac{\Delta S^0}{R} \tag{9}$$

The slope and intercept of $\ln K_c$ versus $1/T$ plot gives the ΔH^0 and ΔS^0, respectively, by assuming temperature independence of the enthalpy and entropy changes. The equilibrium constant K_c can be calculated using the adsorption isotherm equilibrium constants (Langmuir and Freundlich). In the present study, the dimensionless K_c was obtained using the Langmuir equilibrium constant, K_L by the following relation[48,54]:

$$K_c = M_W \cdot 55.5 \cdot 1000 \cdot K_L \tag{10}$$

where M_w is the molecular weight of the adsorbate (g mol^{-1}), and the factor 55.5 is the number of moles of pure water per liter (1000 g L^{-1} divided by 18 g mol^{-1}). Substitution of Eq. (10) into Eq. (9) gives:

$$\ln\left(M_W \cdot 55.5 \cdot 1000 \cdot K_L\right) = \frac{-\Delta H^0}{R}\frac{1}{T} + \frac{\Delta S^0}{R} \tag{11}$$

The thermodynamic parameters were estimated with the help of the linear plot of $\ln K_c$ versus $1/T$ corresponding to the van't Hoff equation with high regression coefficients, R^2 (0.994, 0.988, and 0.984 for TiO_2, SiO_2, and TiO_2/SiO_2, respectively). The

Table 3 – *Thermodynamic parameters for cefdinir adsorption on TiO_2, SiO_2, and TiO_2/SiO_2 adsorbents (Adsorbent loadings = 0.1 g L^{-1}, pH = 4)*

Adsorbent	T (°C)	ΔG^0 (kJ mol^{-1})	ΔH^0 (kJ mol^{-1})	ΔS^0 (J mol^{-1} K^{-1})
TiO_2	25	–27.8	32.6	202.5
	35	–29.8		
	50	–32.8		
SiO_2	25	–29.4	22.6	174.2
	35	–31.1		
	50	–33.7		
TiO_2/SiO_2	25	–13.4	139.1	511.4
	35	–18.5		
	50	–26.2		

parameters are given in Table 3. The negative values of ΔG^0 for all adsorbents at all temperatures indicated the favorable and spontaneous occurrence of the adsorption process. The increase in negative value of ΔG^0 with the increase in temperature confirmed the favorability of the adsorption at high temperatures. The positive values of ΔH^0 showed that the cefdinir adsorption on the adsorbents was endothermic, i.e., the adsorption enhanced with the increase in temperature. In addition, the positive values of ΔS^0 indicated the randomness at the solid-solution interface. The proximity of the thermodynamic parameter values of TiO_2 and SiO_2 pointed to the similarity in their adsorption mechanisms. However, the low values of ΔG^0 and high values of both ΔH^0 and ΔS^0 of TiO_2/SiO_2 showed that its adsorption tendency was lower, and its randomness at the solid-solution interface was higher than that of TiO_2 and SiO_2. The isotherm studies also showed the heterogeneity in the cefdinir adsorption on TiO_2/SiO_2.

Adsorption kinetics

Among the adsorbents studied, TiO_2 was found to be the most effective for the removal of cefdinir from aqueous solution. In order to enhance the adsorption performances of SiO_2 and TiO_2/SiO_2 nanostructures, some surface modifications should be applied to change their surface properties. Therefore, the kinetic study was performed for TiO_2 in order to clarify its adsorption mechanism. The effect of solution temperature on the adsorption behavior was studied kinetically to predict the adsorption uptake and adsorption mechanism. The adsorption mechanism can be described by adsorption reaction and adsorption diffusion models. Adsorption reaction models are based on chemical reaction kinetics. However, adsorption diffusion models can be described on the basis of a number of sequential steps: (1) mass transport in bulk solution phase; (2) diffusion across the liquid film surrounding the adsorbent particle (external or film diffusion); (3) diffusion within the pores and/or along the pore walls of the adsorbent (internal or intraparticle diffusion); (4) adsorption and desorption between the adsorbate and active sites (physisorption or chemisorption). The most widely used adsorption reaction models are pseudo-first-order (PFO) and pseudo-second-order (PSO) reaction models. The first-order rate equation of Lagergren[55] can be expressed as follows[56]:

$$q_t = q_e\left(1 - e^{-k_1 t}\right) \tag{12}$$

where q_t is the amount of adsorbate uptake (mg g^{-1}) at any time t, and k_1 is the pseudo-first-order rate constant (h^{-1}). The second-order rate equation of Blanchard *et al.*[57] can be presented as:

$$q_t = \frac{q_e^2 k_2 t}{1 + k_2 q_e t} \tag{13}$$

where k_2 is the pseudo-second-order rate constant (g mg^{-1} h^{-1}).

The changes in cefdinir uptake with time at different temperatures are given in Fig. 6. The kinetic parameters were estimated using non-linear regression by fitting the experimental data to pseudo-first- and pseudo-second-order model equations. The model parameters are given in Table 4. The thermodynamic studies indicated the endothermic nature of the cefdinir adsorption on TiO_2. The kinetic studies also revealed this result, and for both models, the change in temperature from 25 and 35 °C to 50 °C significantly increased the model rate

Table 4 – *PFO and PSO kinetic model parameters for cefdinir adsorption on TiO_2 at various adsorption temperatures (C_0 = 10 mg L^{-1}, Adsorbent loadings = 1.5 g L^{-1}, pH = 4)*

Temperature (°C)	25	35	50
$q_{e,exp}$ (mg g^{-1})	6.28	7.02	7.28
PFO model			
k_1 (h^{-1})	3.60	3.55	5.28
q_e (mg g^{-1})	5.53	6.32	6.91
R^2	0.871	0.914	0.969
ARD (%)	7.8	6.4	3.7
PSO model			
k_2 (g mg^{-1} h^{-1})	0.96	0.88	1.52
q_e (mg g^{-1})	5.88	6.69	7.16
R^2	0.944	0.973	0.992
ARD (%)	4.8	3.3	2.0

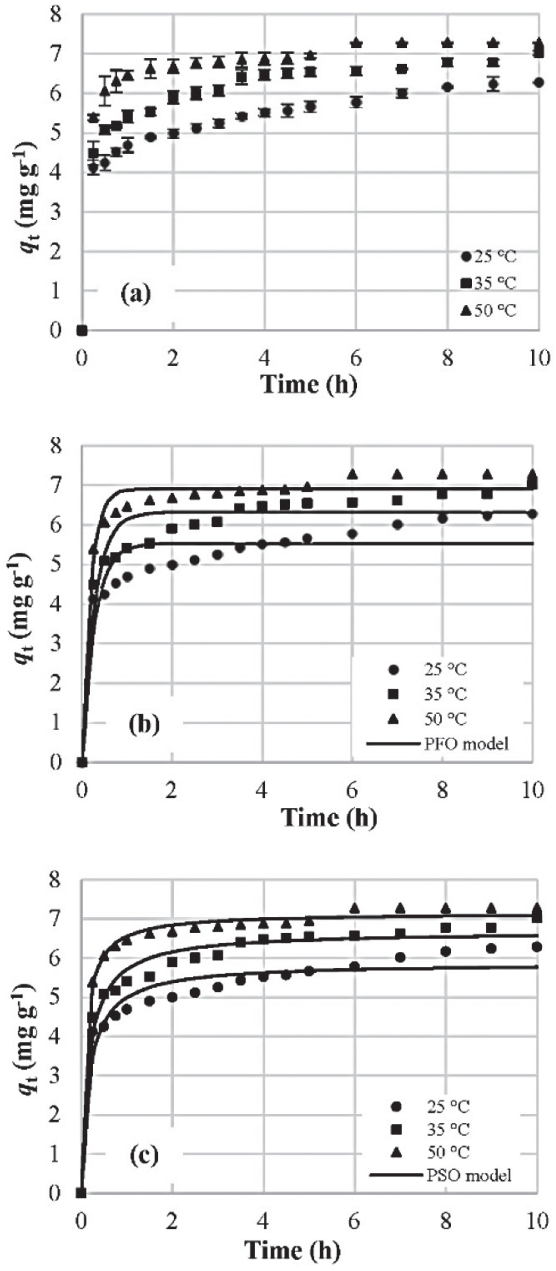

Fig. 6 – *Kinetics of cefdinir adsorption on TiO_2 at various adsorption temperatures (a) experimental data, fitted to (b) PFO, and (c) PSO rate models (C_0 = 10 mg L^{-1}, Adsorbent loadings = 1.5 g L^{-1}, pH = 4)*

constants. The experimental data fitted best with the PSO model equation with high correlation coefficient and low ARD values.

Besides the reaction models, the experimental kinetic data was also evaluated in terms of diffusion mechanisms. Since both the mass transport in the bulk solution phase, and adsorption and desorption between the adsorbate and active sites occur very quickly, they have negligible contribution to the adsorption kinetics. Thus, the diffusion mechanism is generally characterized by liquid film or intraparticle diffusion, where one is predominant over the other and controls the adsorption. The Weber-Morris equation[58] derived from Fick's law for adsorbent diffusing in spherical adsorbent can be used for the determination of the rate-limiting mechanism. In Weber-Morris model, the uptake varies with the square root of adsorption time as[58]:

$$q_t = k_{int}\, t^{1/2} + C \tag{14}$$

where k_{int} is the intraparticle diffusion rate constant (mg g^{-1} h$^{-1/2}$), and C is the apparent thickness of the film boundary layer (mg g^{-1}). If intraparticle diffusion is solely controlling the adsorption as a rate-limiting step, the plot of q_t versus $t^{1/2}$ is a straight line passing through the origin. However, if the plot gives an intercept, then the adsorption kinetics may be controlled by film and intraparticle diffusion simultaneously. The Weber-Morris plot and kinetic parameters of cefdinir uptake at different adsorption temperatures are given in Fig. 7(a) and Table 5, respectively. At all solution temperatures studied, since no lines in the Weber-Morris plots (Fig. 7(a)) passed through the origin, the cefdinir adsorption was not solely controlled by intraparticle diffusion but also affected by film diffusion. At the solution temperature of 25 °C, one linear regime was observed for the adsorption of cefdinir, whereas multi-linear regimes were observed for 35 and 50 °C. The intraparticle diffusion rate constants were determined by linear regression. No significant relation was observed between the intraparticle diffusion rate constants and temperature. However, the intercept C increased with an increase in temperature, indicating the boundary layer effect on adsorption. In addition, for the temperatures of 35 and 50 °C, the intraparticle diffusion constants in the first linear regimes were found to be higher than those in the second regimes. This may be explained by the fast adsorption on the meso- and macropores of the adsorbent following slow adsorption on the micropores, as reported by Zhu *et al.*[49] The plots of the Weber-Morris model (Fig. 7(b)) were predicted using the estimated constants given in Table 5. The size of a cefdinir molecule was estimated with the help of Van der Waals radii approximation, at ca. 0.9 nm. Since the average pore diameter of TiO_2 (2.90 nm) is much larger than the size of a cefdinir molecule, the cefdinir molecule may diffuse easily through the pores of the adsorbent. In order to determine the controlling mechanism (film diffusion or intraparticle diffusion), the experimental data was fitted to the models describing both diffusion mechanisms. The film diffusion mass transfer rate equation presented by Boyd *et al.*[59] was used. This model assumed a liquid film of adsorbate surrounding an adsorbent particle. Due to the difference between the pore size of the adsorbent and molecule size of the adsorbate, the film diffusion may also

Table 5 – *Weber-Morris and film diffusion mass transfer rate kinetic model parameters for cefdinir adsorption on TiO_2 at various adsorption temperatures (C_0 = 10 mg L^{-1}, Adsorbent loadings = 1.5 g L^{-1}, pH = 4)*

Weber-Morris model						
Temperature (°C)	k_{int} (mg g^{-1} $h^{-1/2}$)	C (mg g^{-1})	R^2	k_{int} (mg g^{-1} $h^{-1/2}$)	R^2	ARD (%)
25	0.82	3.81	0.990	–	–	0.9
35	1.05	4.31	0.985	0.56	0.927	0.9
50	0.82	5.55	0.954	0.26	0.963	1.2
Film diffusion mass transfer rate model						
Temperature (°C)	k_{fd} (h^{-1})				R^2	ARD (%)
25	3.55				0.871	7.8
35	3.60				0.914	6.4
50	5.28				0.969	3.7
Homogeneous particle diffusion model						
Temperature (°C)	$D_e \cdot 10^{13}$ (m^2 h^{-1})				R^2	ARD (%)
25	3.59				0.910	5.9
35	3.74				0.947	4.6
50	6.83				0.977	3.1

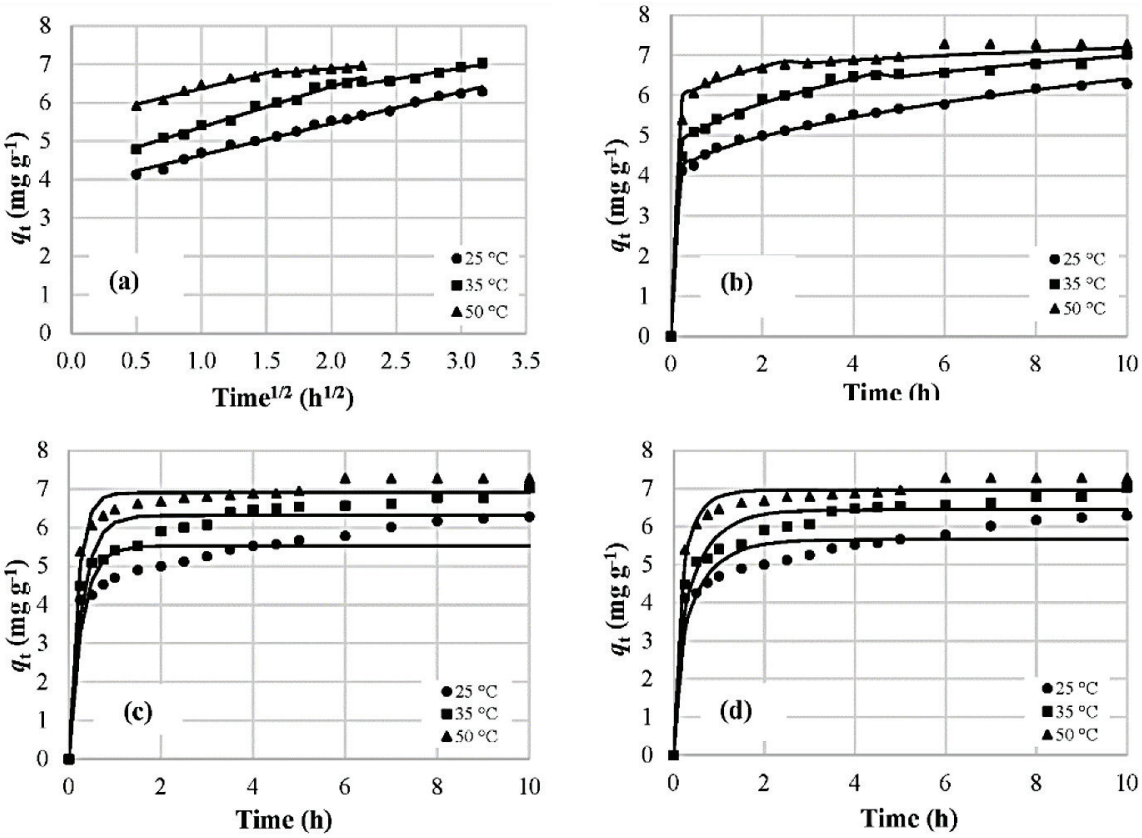

Fig. 7 – *Kinetics of cefdinir adsorption on TiO_2 at various adsorption temperatures fitted to (a) Weber-Morris intraparticle model, predicted using (b) Weber-Morris intraparticle model, (c) Film diffusion mass transfer rate model, (d) Homogeneous particle diffusion model (C_0 = 10 mg L^{-1}, Adsorbent loadings = 1.5 g L^{-1}, pH = 4)*

occur inside the pores between the internal pore surface and bulk solution in the pores. Thus, the kinetic model for the internal film diffusion can be expressed as:

$$\ln\left(1-\frac{q_t}{q_e}\right)=-k_{fd}\,t \qquad (15)$$

where k_{fd} (h^{-1}) is the liquid film diffusion rate constant. The liquid film diffusion constants at different temperatures were estimated from slopes of the $\ln(1–q_t/q_e)$ versus t plots, and are given in Table 5. The liquid film diffusion rate constants increased with the increase in temperature due to the high molecular motion at high temperatures. The adsorption kinetics predicted using the film diffusion mass transfer rate model is given in Fig. 7(c). The model poorly describes the adsorption kinetics of cefdinir on TiO_2. The intraparticle diffusion model was also used to determine the rate-controlling mechanism. The diffusion model by Fick's law in terms of adsorbate uptake, q, is given as:

$$\frac{\partial q}{\partial t}=\frac{1}{r^2}\frac{\partial}{\partial r}\left(r^2 D_e\frac{\partial q}{\partial r}\right) \qquad (16)$$

where r is the radial position, and D_e is the effective diffusion coefficient ($m^2\ h^{-1}$). Eqn. (16) can be solved by the assumptions of (i) homogeneous pore distribution in the spherical adsorbent, (ii) initially no adsorbate at the adsorbent surface, and (iii) constant adsorbate concentration at the surface[49,60]. Thus, solution of Eqn. (16) gives[49,59–61]:

$$\frac{q_t}{q_e}=1-\frac{6}{\pi^2}\sum_{n=1}^{\infty}\frac{1}{n^2}\exp\left(-\frac{n^2\pi^2 D_e\,t}{R^2}\right) \qquad (17)$$

where n is the integer, and R is the radius of the adsorbent (m). The simplified form of Eqn. (17) known as homogeneous particle diffusion model is given as[49,62]:

$$q_t=q_e\left(1-\exp\left(-\frac{\pi^2 D_e}{R^2}t\right)\right)^{1/2} \qquad (18)$$

The effective diffusion coefficient was estimated using the non-linear fit of the experimental data to the model equation given in Eqn. (18). The radius of the TiO_2 adsorbent, which was determined using SEM images, was taken as 1.5 μm. The effective diffusion coefficients and adsorption kinetics predicted from homogeneous particle diffusion model are given in Table 5 and Fig. 7(d). Similar to the internal film diffusion rate constants, the effective diffusion coefficient increased with the increase in temperature, enhancing the rate of molecular motion. The regression coefficients and the ARD% values indicated the suitability of the kinetic model to the experimental data. As may be seen from Table 5 and Fig. 7, among the kinetic models investigated, the cefdinir adsorption kinetics of TiO_2 can be described well by Weber-Morris diffusion model with dominating control mechanism of intraparticle diffusion, and by limited contribution of internal film diffusion.

Reusability of the adsorbent

Because TiO_2 showed the highest adsorptive performance, a reusability study was performed only on this adsorbent. TiO_2 was treated after the adsorption and then reused in the sequential adsorption processes. The treatment was performed by washing the adsorbent with distilled water instead of regeneration. In regeneration studies, in order to remove the residual adsorbate from the surface and/or pore of the adsorbent completely, calcination at high temperatures is usually applied. However, since the synthesis of TiO_2 in the present study included no calcination, which significantly affects the properties of the samples, the adsorbent was not calcined for regeneration. Three reusability cycles were performed and adsorption percentages for the first, second, and third use were obtained as 95, 83, and 72 %, respectively. The reduction in the adsorption percentage after each respective use was presumably due to the unremoved cefdinir molecules which covered and/or blocked the surface and/or pore of the adsorbent TiO_2. In order to prevent this, some chemicals with high cefdinir solubility may be used for washing instead of distilled water.

Conclusion

TiO_2, SiO_2, and TiO_2/SiO_2 nanostructures were used as adsorbents in the removal of cefdinir from aqueous solution. The effects of the adsorption conditions (solution pH, adsorbent dosage, initial adsorbate concentration, and solution temperature) on the adsorption performances were investigated. The changes in both the uptake and adsorption percentage with respect to solution pH indicated the electrostatic interaction between the ionized cefdinir molecule and surface charged nanostructures. The pH and temperature for the highest cefdinir removal were found as 4 and 25 °C for all adsorbents. The large size and high surface area of SiO_2 and TiO_2/SiO_2 led to easy agglomeration of the particles. At high adsorbent dosages, the adsorption percentage decreased because of the decrease in active sites with agglomeration. Thus, the adsorbent dosage passed through a maximum. The optimum adsorbent dosages were estimated at 1.5, 0.5, and 0.75 g L^{-1} for TiO_2, SiO_2, and TiO_2/SiO_2, respectively.

The relation between the adsorbate molecule both in the solution and on the adsorbent surface was defined by the Langmuir and Freundlich isotherm models for TiO_2 and SiO_2, and TiO_2/SiO_2, respectively. The thermodynamic studies indicated favorable and spontaneous occurrence of the adsorption process. Among the adsorbents studied, the adsorption performance of TiO_2 was found to be higher than that of other adsorbents. The PSO reaction model best defined the cefdinir adsorption mechanism of TiO_2. In addition, the adsorption kinetic mechanism of TiO_2 can be described well by Weber-Morris diffusion model by dominating control mechanism of intraparticle diffusion and limited contribution of internal film diffusion. The reusability study also indicated the efficient use of TiO_2 in sequential adsorption processes. Thus, besides the good photocatalytic property of TiO_2, it could be a promising adsorbent for the removal of pharmaceuticals or other organic pollutants from aqueous solution.

ACKNOWLEDGEMENT

This project was supported by the Scientific and Technological Research Council of Turkey (TUBITAK) through Projects 104M255 and 110M451, and the Science, Technology Application, and Research Center of Ege University (EBILTEM) through Project 2012/BIL/027. The author thanks Erdoğanlar Food Industry and Business Company for the rice husk ash, and Sanovel Pharmaceutical Industry and Business Company for cefdinir. The author would like to acknowledge Prof. Dr. Şerife Ş. Helvacı for her valuable advice, Fatma Şahin, Berna Yıldırım and Alper Ayyılmaz for their support.

References

1. *Álvarez-Torrellas, S., Ribeiro, R. S., Gomes, H. T., Ovejero, G., García, J.*, Removal of antibiotic compounds by adsorption using glycerol-based carbon materials, Chem. Eng. J. **296** (2016) 277. doi: https://doi.org/10.1016/j.cej.2016.03.112
2. *Kyzas, G. Z., Fu, J., Lazaridis, N. K., Bikiaris, D. N., Matis, K. A.*, New approaches on the removal of pharmaceuticals from wastewaters with adsorbent materials, J. Mol. Liq. **209** (2015) 87. doi: https://doi.org/10.1016/j.molliq.2015.05.025
3. *Rivera-Utrilla, J., Sanchez-Polo, M., Angeles Ferro-Garcia, M., Prados-Joya, G., Ocampo-Perez, R.*, Pharmaceuticals as emerging contaminants and their removal from water. A review, Chemosphere **93** (2013) 1268. doi: https://doi.org/10.1016/j.chemosphere.2013.07.059
4. *Rakic, V., Rac, V., Krmar, M., Otman, O., Auroux, A.*, The adsorption of pharmaceutically active compounds from aqueous solutions onto activated carbons, J. Hazard. Mater. **282** (2015) 141. doi: https://doi.org/10.1016/j.jhazmat.2014.04.062
5. *Akhtar, J., Amin, N. A. S., Shahzad, K.*, A review on removal of pharmaceuticals from water by adsorption, Desalination and Water Treat. **57** (2016) 12842. doi: https://doi.org/10.1080/19443994.2015.1051121
6. *Al-Khateeb, L. A., Almotiry, S., Salam, M. A.*, Adsorption of pharmaceutical pollutants onto graphene nanoplatelets, Chem. Eng. J. **248** (2014) 191. doi: https://doi.org/10.1016/j.cej.2014.03.023
7. *Lepsy, C. S., Guttendorf, R. J., Kugler, A. R., Smith, D. E.*, Effects of organic anion, organic cation, and dipeptide transport inhibitors on cefdinir in the isolated perfused rat kidney, Antimicrob. Agents Chemother. **47** (2003) 689. doi: https://doi.org/10.1128/AAC.47.2.689–696.2003
8. *Selvi, A., Das, N.*, Nano-bio hybrid system for enhanced degradation of cefdinir using *Candida* sp. SMN04 coated with zero-valent iron nanoparticles, J. Appl. Pharm. Sci. **6** (2016) 009. doi: https://doi.org/10.7324/JAPS.2016.60902
9. *Cho, H. J., Jee, J. P., Kang, J. Y., Shin, D. Y., Choi, H. G., Maeng, H. J., Cho, K. H.*, Cefdinir solid dispersion composed of hydrophilic polymers with enhanced solubility, dissolution, and bioavailability in rats, Molecules **22** (2017) 1. doi: https://doi.org/10.3390/molecules22020280
10. *Duan, H.*, Study on the treatment process of wastewater from cephalosporin production, J. Sustainable Dev. **2** (2009) 132.
11. *Collado, S., Quero, D., Laca, A., Díaz, M.*, Efficiency and sensitivity of the wet oxidation/biological steps in coupled pharmaceutical wastewater treatment, Chem. Eng. J. **234** (2013) 484. doi: https://doi.org/10.1016/j.cej.2013.07.075
12. *Li, W., Niu, Q., Zhang, H., Tian, Z., Zhang, Y., Gao, Y., Li, Y.-Y., Nishimura, O., Yang, M.*, UASB treatment of chemical synthesis-based pharmaceutical wastewater containing rich organic sulfur compounds and sulfate and associated microbial characteristics, Chem. Eng. J. **260** (2015) 55. doi: https://doi.org/10.1016/j.cej.2014.08.085
13. *Mowla, A., Mehrvar, M., Dhib, R.*, Combination of sonophotolysis and aerobic activated sludge processes for treatment of synthetic pharmaceutical wastewater, Chem. Eng. J. **255** (2014) 411. doi: https://doi.org/10.1016/j.cej.2014.06.064
14. *Selvi, A., Das, D., Das, N.*, Potentiality of yeast candida sp. SMN04 for degradation of cefdinir, a cephalosporin antibiotic: Kinetics, enzyme analysis and biodegradation pathway, Environ. Technol. **36** (2015) 3112. doi: https://doi.org/10.1080/09593330.2015.1054318
15. *Ahmadzadeh, S., Asadipour, A., Yoosefian, M., Dolatabadi, M.*, Improved electrocoagulation process using chitosan for efficient removal of cefazolin antibiotic from hospital wastewater through sweep flocculation and adsorption: Kinetic and isotherm study, Desalination Water Treat. **92** (2017) 160. doi: https://doi.org/10.5004/dwt.2017.21492
16. *Serna-Galvis, E. A., Berrio-Perlaza, K. E., Torres-Palma, R. A.*, Electrochemical treatment of penicillin, cephalosporin, and fluoroquinolone antibiotics via active chlorine: Evaluation of antimicrobial activity, toxicity, matrix, and their correlation with the degradation pathways, Environ. Sci. Pollut. Res. Int. **24** (2017) 23771. doi: https://doi.org/10.1007/s11356-017-9985-2
17. *Yang, B., Zuo, J., Gan, L., Yu, X., Liu, F., Tang, X., Wang, Y.*, Advanced treatment of cephalosporin pharmaceutical wastewater by nano-coated electrode and perforated electrode, J. Environ. Sci. Health, Part A **49** (2014) 1258. doi: https://doi.org/10.1080/10934529.2014.910044

18. *Yang, B., Zuo, J., Li, P., Wang, K., Yu, X., Zhang, M.*, Effective ultrasound electrochemical degradation of biological toxicity and refractory cephalosporin pharmaceutical wastewater, Chem. Eng. J. **287** (2016) 30. doi: https://doi.org/10.1016/j.cej.2015.11.033
19. *Perini, J. A. L., Tonetti, A. L., Vidal, C., Montagner, C. C., Nogueira, R. F. P.*, Simultaneous degradation of ciprofloxacin, amoxicillin, sulfathiazole and sulfamethazine, and disinfection of hospital effluent after biological treatment via photo-fenton process under ultraviolet germicidal irradiation, Appl. Catal. B **224** (2018) 761. doi: https://doi.org/10.1016/j.apcatb.2017.11.021
20. *Reina, A. C., Martinez-Piernas, A. B., Bertakis, Y., Brebou, C., Xekoukoulotakis, N. P., Aguera, A., Sanchez Perez, J. A.*, Photochemical degradation of the carbapenem antibiotics imipenem and meropenem in aqueous solutions under solar radiation, Water Res. **128** (2018) 61. doi: https://doi.org/10.1016/j.watres.2017.10.047
21. *Serna-Galvis, E. A., Silva-Agredo, J., Giraldo, A. L., Florez-Acosta, O. A., Torres-Palma, R. A.*, Comparative study of the effect of pharmaceutical additives on the elimination of antibiotic activity during the treatment of oxacillin in water by the photo-Fenton, TiO_2-photocatalysis and electrochemical processes, Sci. Total Environ. **541** (2016) 1431. doi: https://doi.org/10.1016/j.scitotenv.2015.10.029
22. *Kim, J. R., Kan, E.*, Heterogeneous photocatalytic degradation of sulfamethoxazole in water using a biochar-supported TiO_2 photocatalyst, J. Environ. Manage. **180** (2016) 94. doi: https://doi.org/10.1016/j.jenvman.2016.05.016
23. *Kanakaraju, D., Kockler, J., Motti, C. A., Glass, B. D., Oelgemöller, M.*, Titanium dioxide/zeolite integrated photocatalytic adsorbents for the degradation of amoxicillin, Appl. Catal. B **166–167** (2015) 45. doi: https://doi.org/10.1016/j.apcatb.2014.11.001
24. *Dao, T. H., Tran, T. T., Nguyen, V. R., Pham, T. N. M., Vu, C. M., Pham, T. D.*, Removal of antibiotic from aqueous solution using synthesized TiO_2 nanoparticles: Characteristics and mechanisms, Environ. Earth Sci. **77** (2018). doi: https://doi.org/10.1007/s12665-018-7550-z
25. *Ali, M. E. M., Abd El-Aty, A. M., Badawy, M. I., Ali, R. K.*, Removal of pharmaceutical pollutants from synthetic wastewater using chemically modified biomass of green alga *Scenedesmus obliquus*, Ecotoxicol. Environ. Saf. **151** (2018) 144. doi: https://doi.org/10.1016/j.ecoenv.2018.01.012
26. *Arshadi, M., Mousavinia, F., Abdolmaleki, M. K., Amiri, M. J., Khalafi-Nezhad, A.*, Removal of salicylic acid as an emerging contaminant by a polar nano-dendritic adsorbent from aqueous media, J. Colloid Interface Sci. **493** (2017) 138. doi: https://doi.org/10.1016/j.jcis.2017.01.017
27. *Dong, X., He, L., Hu, H., Liu, N., Gao, S., Piao, Y.*, Removal of 17β-estradiol by using highly adsorptive magnetic biochar nanoparticles from aqueous solution, Chem. Eng. J. **352** (2018) 371. doi: https://doi.org/10.1016/j.cej.2018.07.025
28. *Habibi, A., Belaroui, L. S., Bengueddach, A., López Galindo, A., Sainz Díaz, C. I., Peña, A.*, Adsorption of metronidazole and spiramycin by an Algerian palygorskite. Effect of modification with tin, Microporous Mesoporous Mater. **268** (2018) 293. doi: https://doi.org/10.1016/j.micromeso.2018.04.020
29. *Naeimi, S., Faghihian, H.*, Application of novel metal organic framework, MIL-53(Fe) and its magnetic hybrid: For removal of pharmaceutical pollutant, doxycycline from aqueous solutions, Environ. Toxicol. Pharmacol. **53** (2017) 121. doi: https://doi.org/10.1016/j.etap.2017.05.007
30. *Sikarwar, S., Jain, R.*, Adsorption kinetics studies of an anti-inflammatory drug Mesalamine using unsaturated polyester resin (UPR), J. Mol. Liq. **224** (2016) 219. doi: https://doi.org/10.1016/j.molliq.2016.09.107
31. *Yu, F., Ma, J., Bi, D.*, Enhanced adsorptive removal of selected pharmaceutical antibiotics from aqueous solution by activated graphene, Environ. Sci. Pollut. Res. Int. **22** (2015) 4715. doi: https://doi.org/10.1007/s11356-014-3723-9
32. *Ounnar, A., Bouzaza, A., Favier, L., Bentahar, F.*, Macrolide antibiotics removal using a circulating TiO_2-coated paper photoreactor: Parametric study and hydrodynamic flow characterization, Water Sci. Technol. **73** (2016) 2627. doi: https://doi.org/10.2166/wst.2016.096
33. *Mestre, A. S., Pires, R. A., Aroso, I., Fernandes, E. M., Pinto, M. L., Reis, R. L., Andrade, M. A., Pires, J., Silva, S. P., Carvalho, A. P.*, Activated carbons prepared from industrial pre-treated cork: Sustainable adsorbents for pharmaceutical compounds removal, Chem. Eng. J. **253** (2014) 408. doi: https://doi.org/10.1016/j.cej.2014.05.051
34. *Xiao, G., Wen, R., Liu, A., He, G., Wu, D.*, Adsorption performance of salicylic acid on novel resin with distinctive double pore structure, J. Hazard. Mater. **329** (2017) 77. doi: https://doi.org/10.1016/j.jhazmat.2017.01.030
35. *Domínguez-Vargas, J. R., Gonzalez, T., Palo, P., Cuerda-Correa, E. M.*, Removal of carbamazepine, naproxen, and trimethoprim from water by amberlite xad-7: A kinetic study, CLEAN – Soil, Air, Water **41** (2013) 1052. doi: https://doi.org/10.1002/clen.201200245
36. *Rakić, V., Rajić, N., Daković, A., Auroux, A.*, The adsorption of salicylic acid, acetylsalicylic acid and atenolol from aqueous solutions onto natural zeolites and clays: Clinoptilolite, bentonite and kaolin, Microporous Mesoporous Mater. **166** (2013) 185. doi: https://doi.org/10.1016/j.micromeso.2012.04.049
37. *Bui, T. X., Choi, H.*, Adsorptive removal of selected pharmaceuticals by mesoporous silica SBA-15, J. Hazard. Mater. **168** (2009) 602. doi: https://doi.org/10.1016/j.jhazmat.2009.02.072
38. *Curry, D. E., Andrea, K. A., Carrier, A. J., Nganou, C., Scheller, H., Yang, D., Youden, B., Zhang, Y., Nicholson, A., Cui, S., Oakes, K. D., MacQuarrie, S. L., Lu, M., Zhang, X.*, Surface interaction of doxorubicin with anatase determines its photodegradation mechanism: Insights into removal of waterborne pharmaceuticals by TiO_2 nanoparticles, Environ. Sci. Nano **5** (2018) 1027. doi: https://doi.org/10.1039/c7en01171g
39. *Wang, J., Liu, R., Yin, X.*, Adsorptive removal of tetracycline on graphene oxide loaded with titanium dioxide composites and photocatalytic regeneration of the adsorbents, J. Chem. Eng. Data **63** (2018) 409. doi: https://doi.org/10.1021/acs.jced.7b00816
40. *Cheng, G., Xu, F., Xiong, J., Tian, F., Ding, J., Stadler, F. J., Chen, R.*, Enhanced adsorption and photocatalysis capability of generally synthesized TiO_2-carbon materials hybrids, Adv. Powder Technol. **27** (2016) 1949. doi: https://doi.org/10.1016/j.apt.2016.06.026
41. *Klapiszewski, Ł., Siwińska-Stefańska, K., Kołodyńska, D.*, Preparation and characterization of novel TiO_2/lignin and TiO_2-SiO_2/lignin hybrids and their use as functional biosorbents for Pb(II), Chem. Eng. J. **314** (2017) 169. doi: https://doi.org/10.1016/j.cej.2016.12.114
42. *Liu, S., Lim, M., Amal, R.*, TiO_2-coated natural zeolite: Rapid humic acid adsorption and effective photocatalytic regeneration, Chem. Eng. Sci. **105** (2014) 46. doi: https://doi.org/10.1016/j.ces.2013.10.041

43. *Wang, Y., Xing, Z., Li, Z., Wu, X., Wang, G., Zhou, W.*, Facile synthesis of high-thermostably ordered mesoporous TiO_2/SiO_2 nanocomposites: An effective bifunctional candidate for removing arsenic contaminations, J. Colloid Interface Sci. **485** (2017) 32.
doi: https://doi.org/10.1016/j.jcis.2016.09.022
44. *Smirnova, I., Mamic, J., Arlt, W.*, Adsorption of drugs on silica aerogels, Langmuir **19** (2003) 8521.
doi: https://doi.org/10.1021/la0345587
45. *Selvi, A., Das, D.*, Remediation of cefdinir from aqueous solution using pretrated dead yeast *Candida* sp. SMN04 as potential adsorbent: An equilibrium, kinetics and thermodynamic studies, Der Pharmacia Lettre **7** (2015) 74.
46. *Yener, H. B., Helvacı, Ş. Ş.*, Effect of synthesis temperature on the structural properties and photocatalytic activity of TiO_2/SiO_2 composites synthesized using rice husk ash as a SiO_2 source, Sep. Purif. Technol. **140** (2015) 84.
doi: https://doi.org/10.1016/j.seppur.2014.11.013
47. *Sanli, N., Sanli, S., Sızır, U., Gumustas, M., Ozkan, S. A.*, Determination of pK_a values of cefdinir and cefixime by LC and spectrophotometric methods and their analysis in pharmaceutical dosage forms, Chromatographia **73** (2011) 1171.
doi: https://doi.org/10.1007/s10337-011-2013-7
48. *Tran, H. N., You, S. J., Hosseini-Bandegharaei, A., Chao, H. P.*, Mistakes and inconsistencies regarding adsorption of contaminants from aqueous solutions: A critical review, Water Res. **120** (2017) 88.
doi: https://doi.org/10.1016/j.watres.2017.04.014
49. *Zhu, Q., Moggridge, G. D., D'Agostino, C.*, Adsorption of pyridine from aqueous solutions by polymeric adsorbents MN 200 and MN 500. Part 2: Kinetics and diffusion analysis, Chem. Eng. J. **306** (2016) 1223.
doi: https://doi.org/10.1016/j.cej.2016.07.087
50. *Langmuir, I.*, The adsorption of gases on plane surfaces of glass, mica and platinum, J. Am. Chem. Soc. **49** (1918) 1361.
doi: https://doi.org/10.1021/ja02242a004
51. *Freundlich, H.*, Adsorption in solution, Zeitschrift für Physikalische Chemie **57** (1906) 384.
doi: https://doi.org/10.1515/zpch-1907-5723
52. *Behnajady, M., Yavari, S., Modirshahla, N.*, Investigation on adsorption capacity of TiO_2-P25 nanoparticles in the removal of a mono-azo dye from aqueous solution: A comprehensive isotherm analysis, Chem. Ind. Chem. Eng. Q. **20** (2014) 97.
doi: https://doi.org/10.2298/CICEQ120610105B
53. *Padmavathy, K. S., Madhu, G., Haseena, P. V.*, A study on effects of pH, adsorbent dosage, time, initial concentration and adsorption isotherm study for the removal of hexavalent chromium (Cr(VI)) from wastewater by magnetite nanoparticles, Procedia Technol. **24** (2016) 585.
doi: https://doi.org/10.1016/j.protcy.2016.05.127
54. *Tran, H. N., You, S.-J., Chao, H.-P.*, Thermodynamic parameters of cadmium adsorption onto orange peel calculated from various methods: A comparison study, J. Environ. Chem. Eng. **4** (2016) 2671.
doi: https://doi.org/10.1016/j.jece.2016.05.009
55. *Lagergren, S.*, About the theory of so-called adsorption of soluble substances, Kungliga Svenska Vetenskapsakademiens Handlingar **24** (1898) 1.
56. *Ho, Y. S., McKay, G.*, A comparison of chemisorption kinetic models applied to pollutant removal on various sorbents, Process Saf. Environ. Prot. **76** (1998) 332.
doi: https://doi.org/957±5820/98/$10.00+0.00
57. *Blanchard, G., Maunaye, M., Martin, G.*, Removal of heavy metals from waters by means of natural zeolites, Water Res. **18** (1984) 1501.
doi: https://doi.org/10.1016/0043-1354(84)90124-6
58. *Weber, W. J., Morris, J. C.*, Kinetics of adsorption on carbon from solution, J. Sanitary Eng. Div. **89** (1963) 31.
59. *Boyd, G. E., Adamson, A. W., Myers, L. S.*, The exchange adsorption of ions from aqueous solutions by organic zeolites. II. Kinetics, J. Am. Chem. Soc. **69** (1947) 2836.
doi: https://doi.org/10.1021/ja01203a066
60. *Qiu, H., Lv, L., Pan, B.-c., Zhang, Q.-j., Zhang, W.-m., Zhang, Q.-x.*, Critical review in adsorption kinetic models, J. Zhejiang Univ. Sci. A **10** (2009) 716.
61. *Eagle, S., Scott, J. W.*, Liquid phase adsorption equilibria and kinetics, Ind. Eng. Chem. **42** (1950) 1287.
doi: https://doi.org/10.1021/ie50487a016
62. *Vermeulen, T.*, Theory for irreversible and constant-pattern solid diffusion, Ind. Eng. Chem. **45** (1953) 1664.
doi: https://doi.org/10.1021/ie50524a025